Magnetic Resonance Imaging 68 (2020) 106–112

Contents lists available at ScienceDirect

Magnetic Resonance Imaging

journal homepage: www.elsevier.com/locate/mri

Original contribution

Prediction of survival and progression in glioblastoma patients using temporal perfusion changes during radiochemotherapy

Christopher Larsson[a,b,*], Inge Groote[b], Jonas Vardal[a,b], Magne Kleppestø[a,b], Audun Odland[c], Petter Brandal[a,d], Paulina Due-Tønnessen[a,e], Sigrun S. Holme[e], Tuva R. Hope[b], Torstein R. Meling[a,f], Erik Fosse[a,b], Kyrre E. Emblem[b], Atle Bjørnerud[b,g]

[a] Faculty of Medicine, University of Oslo, Oslo, Norway
[b] The Intervention Centre, Oslo University Hospital, Oslo, Norway
[c] Department of Radiology, Stavanger University Hospital, Stavanger, Norway
[d] Department of Oncology, Oslo University Hospital, Oslo, Norway
[e] Department of Radiology, Oslo University Hospital, Oslo, Norway
[f] Department of Neurosurgery, Oslo University Hospital, Oslo, Norway
[g] Department of Physics, University of Oslo, Oslo, Norway

A B S T R A C T

Background: The aim of this study was to investigate changes in structural magnetic resonance imaging (MRI) according to the RANO criteria and perfusion- and permeability related metrics derived from dynamic contrast-enhanced MRI (DCE) and dynamic susceptibility contrast MRI (DSC) during radiochemotherapy for prediction of progression and survival in glioblastoma.

Methods: Twenty-three glioblastoma patients underwent biweekly structural and perfusion MRI before, during, and two weeks after a six weeks course of radiochemotherapy. Temporal trends of tumor volume and the perfusion-derived parameters cerebral blood volume (CBV) and blood flow (CBF) from DSC and DCE, in addition to contrast agent capillary transfer constant (K^{trans}) from DCE, were assessed. The patients were separated in two groups by median survival and differences between the two groups explored. Clinical- and MRI metrics were investigated using univariate and multivariate survival analysis and a predictive survival index was generated.

Results: Median survival was 19.2 months. A significant decrease in contrast-enhancing tumor size and CBV and CBF in both DCE- and DSC-derived parameters was seen during and two weeks past radiochemotherapy ($p < 0.05$). A 10%/30% increase in K^{trans}/CBF two weeks after finishing radiochemotherapy resulted in significant shorter survival (13.9/16.8 vs. 31.5/33.1 months; $p < 0.05$). Multivariate analysis revealed an index using change in K^{trans} and relative CBV from DSC significantly corresponding with survival time in months ($r^2 = 0.843$; $p < 0.001$).

Conclusions: Significant temporal changes are evident during radiochemotherapy in tumor size (after two weeks) and perfusion-weighted MRI-derived parameters (after four weeks) in glioblastoma patients. While DCE-based metrics showed most promise for early survival prediction, a multiparametric combination of both DCE- and DSC-derived metrics gave additional information.

1. Introduction

Glioblastoma (GBM) is the most common primary brain cancer in adults. Prognosis is dire, with an average overall survival (OS) of 12–15 months [1]. The OS range is, however, wide and some patients respond beneficial to therapy and have a two-year OS of 20–25%, making early and correct prognosis challenging [1,2]. Accurate prognosis is preferred by cancer patients [3], in addition, early prognostic biomarkers are warranted for timely change of therapy in cases showing tumor recurrence and treatment failure.

The Response Assessment in Neuro-Oncology (RANO) criteria, considered to be the gold standard in GBM assessment, are based on the visual radiological evaluation of structural image series [4]. These criteria include estimating changes in MRI-based measures of tumor size, measured on two-dimensional structural T1-weighted (T1w) and T2-weighted (T2w) or Fluid Attenuated Inversion Recovery (FLAIR)-weighted images, in conjunction with corticosteroid use and clinical deterioration [4]. Disease response is grouped into four categories: complete response, partial response, stable disease, and progressive disease. Concerns about the limited ability of structural measurements to reflect pathologic heterogeneity and predict OS have led to an interest in more sophisticated MRI tools [5,6]. Perfusion-weighted MRI techniques are used increasingly in the assessment of GBMs and most tumor protocols now include either dynamic contrast-enhanced MRI,

* Corresponding author at: Oslo University Hospital, Sognsvannveien 20, 0372 Oslo, Norway.
E-mail address: larsch@ous-hf.no (C. Larsson).

https://doi.org/10.1016/j.mri.2020.01.012
Received 12 September 2019; Received in revised form 10 January 2020; Accepted 23 January 2020
0730-725X/ © 2020 The Authors. Published by Elsevier Inc. This is an open access article under the CC BY license (http://creativecommons.org/licenses/BY/4.0/).

(DCE) and/or dynamic susceptibility contrast MRI (DSC) [7]. Perfusion imaging for prognostics is promising in several studies [8–10]. However, there is no consensus on how to best perform this assessment during conventional therapy [11]. Studies vary with respect to imaging time-point relative to treatment, statistical analysis, and the metrics investigated. Furthermore, few have systematically investigated differences and similarities between DSC and DCE in terms of their ability to predict outcome [10].

To this end, we hypothesized that perfusion derived metrics will help improve the prediction of OS in GBM patients, compared to conventional volumetric or radiologic assessment by the RANO criteria alone. Furthermore, our study aimed to assess the temporal trends of estimated parameters derived from DCE and DSC imaging and differences in their predictive value.

2. Methods

2.1. Patient population

Patients with histologically confirmed high-grade glioma (grade III and IV) operated at our institution between May 2010 and May 2012 were eligible for inclusion in this prospective study at start of radiochemotherapy treatment. Approval from the regional ethics committee and written informed consent was obtained from all patients before imaging start. Exclusion criteria were impaired renal function (estimated glomerular filtration rate (eGFR) <60 ml/min), claustrophobia and artifacts from surgical clips near the area of interest. A series of 23 patients were included and available for the final analysis; for key demographics see Table 1. Treatment included surgery when possible, followed by stereotactic radiotherapy approximately four weeks after surgery with concomitant and adjuvant chemotherapy with temozolomide according to the standard treatment protocol proposed by Stupp et al. [2]. Imaging was performed immediately before the start of radiochemotherapy, every second week during this treatment, as well as two weeks after treatment. At each imaging time-point, clinical assessment was done using the Karnofsky performance status (KPS) [12].

2.2. MRI

Imaging was performed using a 3 Tesla Philips Achieva (Philips Medical Systems, Best, The Netherlands), using an eight-channel head coil. Structural imaging included a 3D FLAIR, (echo time (TE)/repetition time (TR)/inversion time (TI) (ms) = 424/8000/2400, voxel size $1.07 \times 1.07 \times 0.6$ mm^3, matrix 224×224, 300 slices); a 3D T1w gradient echo (GRE) before and after contrast agent injection (TE/TR = 2.3/5.1 ms, voxel size $1 \times 1 \times 1$ mm^3, matrix 256×232, 190 slices).

Perfusion-weighted imaging: DCE were acquired using a 3D saturation recovery (SR) GRE sequence (TE/TR/flip angle (FA) = 2.5/8.2 ms/26°, voxel size $2 \times 2 \times 4$ mm^3 (interpolated to $1.8 \times 1.8 \times 4$ mm^3), matrix 120×120, 11 slices), a SENSE factor of 2 was used [13]. Each slice was acquired after application of a non-selective saturation prepulse with a saturation time delay (TD). Centric phase ordering was used so that centre of k-space was recorded at time TD. TD/sampling interval was 80 ms/3.4 s (first seven subjects) in a double-echo sequence and 50 ms/2.1 s in the remaining subjects, giving a total of 100 or 150 dynamic images respectively [14]. For the DSC a 2D spin echo (SE) echo planar imaging (EPI) (TE/TR = 70/1349 ms, voxel size $1.88 \times 1.88 \times 4.0$ mm^3, matrix 120×120, 13 slices, sampling interval of 1.33 s) sequence was used. DCE was performed before DSC, and 0.1 mmol/kg body weight gadobutrol (Gadovist®, Bayer Schering Pharma AG, Berlin, Germany) was injected after baseline imaging for both DCE and DSC using a power injector, at a rate of 3 mL/s and 5 mL/s respectively, immediately followed by a 20 mL saline flush.

2.3. Image preprocessing and data analysis

2.3.1. Co-registration and region-of-interest creation

Co-registration was performed using SPM8 in a hierarchic manner. Pre-treatment non-contrast T1w image sets served as reference, and non-contrast T1w images from each time-point were co-registered to the reference image. Contrast enhanced T1w- and FLAIR images were registered to already registered non-contrast T1w images. DCE-data was registered to contrast-enhanced T1w images and DSC-data to FLAIR images for optimal results. The framework is shown in Supplementary Fig. 1. Two regions-of-interest (ROIs) were generated using a semi-automatic method previously described [15]. In short, a contrast-enhancing tumor (CET) ROI was defined from hyper-intense regions in the contrast enhanced T1w images. Thick linear enhancement in the contrast enhanced T1w images (>2 pixels thick) was included in the ROIs as this has shown the same prognostic significance as nodular enhancement early post operatively [16]. A non-enhancing tumor (NET) ROI was defined from regions of high signal intensity in the FLAIR images. The CET was subtracted from the NET to avoid overlapping ROIs. All auto-generated ROIs were edited and approved by a radiologist (4 years of experience). ROIs smaller than 0.5 mL were excluded from the analysis.

2.3.2. Visual assessments

Radiographic progression-free survival (PFS) was defined as time to progressive disease according to the RANO criteria [4]. Three radiologists (4–22 years of experience) made a consensus agreement for each patient case. In addition to the four RANO categories, a fifth category – pseudoprogression - was included. Pseudoprogression was defined by new or growing contrast enhancing lesions where the radiographic findings were stable for more than six months and later decreased in size or was confirmed by surgery (one patient). Volumes of CET and NET, in addition to volumetric change from baseline, were estimated from the structural images.

Table 1
Key demographics of all patients and for the two survival groups based on median split. Median values and estimated 95% confidence intervals shown in parenthesis. KPS = Karnofsky Performance Score, CET = Contrast enhanced tumor, NET = non-enhanced tumor, GTR = gross total resection, STR = sub-total resection.

Characteristics	All patients (n = 23)		Overall survival >19.1 months (n = 11)		Overall survival <19.1 months (n = 12)	
Age	56.2	(49.5–62.6)	54.5	(32.7–64.3)	59.5	(49.5–64.8)
Sex (female/male)	6/17		2/9		4/8	
KPS score at baseline	100		100		100	
Progression free survival	7.1	(4.0–20.8)	29.8	(9.8–45.3)	2.45	(0–5.3)
Overall survival (months)	19.2	(13.6–33.6)	38.4	(29.0–55.1)	13.4	(9.9–15.8)
CET at baseline (ml)	5.8	(4.4–11.1)	5.8	(1.3–18.0)	6.63	(3.2–29.0)
NET at baseline (ml)	15.3	(3.9–37.5)	9.3	(1.6–85.6)	33.0	(3.2–57.5)
Surgery (Biopsy/STR/GTR)	1/8/14		1/3/7		0/5/7	

Key demographics of all patients and for the two survival groups based on median split. Median values and estimated 95% confidence intervals shown in parenthesis. KPS = Karnofsky Performance Score, CET = Contrast enhanced tumor, NET = non-enhanced tumor, GTR = gross total resection, STR = sub-total resection.

2.3.3. Perfusion processing

The extended two-compartment Tofts model was used for the DCE analysis, yielding statistical parametric maps of the unidirectional contrast agent capillary transfer constant (K^{trans}) and plasma volume (v_p) [17]. A fixed baseline T_1 of 1490 ms across all patients was used for further analysis [18,19]. Patient-specific carry-on arterial input functions (AIFs) obtained from the baseline scan was used for both DCE and DSC analysis at every time-point as previously described [20]. In addition to parametric maps of K^{trans} and v_p, CBF from all time-points (CBF_{T1}) was also estimated from the DCE data. An example of the model fit and the residual function from the DCE is shown in Supplementary Fig. 2The DSC series was corrected for geometric EPI distortions [21], and parametric maps representing CBF (CBF_{T2}) and CBV (CBV_{T2}) were generated [22]. Absolute measures of CBF_{T2} and CBV_{T2} using a patient-specific carry-on AIF from the first scan [20], as well as values relative to normal appearing grey- and white matter ($rCBF_{T2}$ and $rCBV_{T2}$) were estimated from the DSC data [23]. CBF was estimated based on the same method in the DCE and DSC series [24]. All image analysis was performed using the nordicICE analysis package (NordicNeuroLab AS, Bergen, Norway).

2.3.4. Statistical analysis

Median OS and PFS, from the date of radiochemotherapy start, were calculated from Kaplan-Meier plots and the subjects were divided according to a median split in two groups. Median and 90-percentile values of all perfusion parameters were investigated for absolute values and the percentage change from the baseline scan (δ), for both ROIs. Temporal change from the baseline examination in all patients was assessed using Wilcoxon signed-rank test, with Holm-Bonferroni corrections for multiple comparisons. Differences in the two survival groups were assessed by Mann-Whitney *U* test. Receiver operating characteristics (ROC) curves were investigated for significant parameters from the Mann-Whitney U test and dichotomized based upon Youdens index [25]. Parameter correlation was assessed using Spearman's correlation. Log-rank test and Kaplan-Meier plots for OS were then generated based on the cut-off values from the ROC curve analysis. In an effort to accurately predict OS, in compliance with earlier published work, a survival index was produced by combining parameters from DCE and DSC [26]. Cox proportional hazards analysis using age as a time dependent covariate and changes in log-transformed K^{trans} and $rCBV_{T2}$ from baseline to week eight was performed. Using the sum of the estimated regression coefficients β for each parameter an index for each patient was calculated using the following formula and correlated to OS [26].

$$Survival\ Index = \beta 1\ x\ \delta Ktrans + \beta 2\ x\ \delta rCBV + \beta 3\ x\ age$$

The predictive value of the index was assessed using a concordance index [27]. Findings were considered significant if $p < 0.05$. All statistical analyses were performed in Statistical Package of the Social Sciences (SPSS) v.22 (IBM Corporation, New York, USA).

3. Results

Median OS and PFS for all patients were 19.2 (2.0–36.3) and 8.9 (3.8–14.0) months, respectively. Evolution of RANO grade, PFS and OS for each patient is shown in Fig. 1. A strong correlation between PFS and OS was found ($r2 = 0.843$; $p < 0.001$). Patients with radiographic progression during the first 12 months had a significantly shorter OS (13.5 months; 12.8–14.3) than those without progression (40 months; 34.0–47.0; $p < 0.001$).

Temporal changes in tumor sub-volumes (CET and NET), DCE and DSC parameters for all patients during- and two weeks past radiochemotherapy, are shown in Fig. 2a and Supplementary Fig. 3. CET decreased at all time-points ($p < 0.05$). NET volume showed a significant increase in absolute and relative volume at the second and third time-point respectively ($p < 0.05$). 90 percentile values of CBF_{T1} and v_p decreased two weeks past the end of radiochemotherapy in both CET and NET ($p < 0.05$). Significant decreases in $rCBF_{T2}$ and $rCBV_{T2}$ were evident at four weeks in both median and 90-percentile values in CET ($p < 0.05$). Representative images of the evolution of structural volume and perfusion metrics in two sample patients are shown in Fig. 3.

The temporal evolution of δ-values in the two survival groups is shown in Fig. 2b and Supplementary Fig. 4. Both δ CBF_{T1} and K^{trans} in CET showed increasing differences during treatment. Patients with stable or decreasing CBF_{T1}/K^{trans} at two weeks after radiochemotherapy had prolonged survival of 33.1/31.5 months compared to patients with increasing values (16.8/13.9 months; $p = 0.036/0.016$). ROC curve analysis revealed a cut-off value for δ CBF_{T1} and δ K^{trans} of 10% and 30% from the Youden index ($p = 0.016$ and $p = 0.021$). The Kaplan Meier plots of both parameters are shown in Fig. 4a along with two sample patients (Fig. 4b) and parameter histograms (Fig. 4c). δ K^{trans} and CBF_{T1} in CET correlated significantly at all time-points ($r^2 > 0.847$; $p < 0.001$).

Univariate Cox regression revealed age as a significant predictor for OS ($p = 0.013$). Other known clinical predictors including tumor volume, KPS, and surgical resection were not found to be significant. No continuous parameter was found significant in the univariate analysis. Multiparametric Cox regression of log-transformed δ K^{trans} and δ $rCBV_{T2}$ were significant ($p = 0.028$ and $p = 0.025$) for OS. The index was significantly negatively correlated with OS ($r^2 = 0.843$; $p < 0.001$). A strong concordance with a Harrels C score of 0.881 was found for the index. All beta coefficients were positive, signifying that higher age, increasing K^{trans} and increase in $rCBV_{T2}$ from baseline were associated with shorter OS.

4. Discussion

This study demonstrates a decrease in CET volume and a decrease in DSC derived $CBF_{T2,}$ and CBV_{T2} in GBM patients during- and two weeks after radiochemotherapy. In addition, the prognostic value of K^{trans} and CBF_{T1} from DCE in CET was superior to the DSC-derived parameters. An index of age and log-transformed K^{trans} and $rCBV_{T2}$ showed strong correlation with survival.

In agreement with previous studies, PFS and OS varied much within the patient population (Fig. 1). However, PFS is not a good marker for survival prediction [26]. According to the RANO criteria, progression can only be evaluated three months after the end of radiochemotherapy at the earliest due to pseudoprogression [4]. Pseudoprogression occurs in 20–30% of patients during radiochemotherapy, effectively making PFS unreliable as a predictive biomarker until pseudoprogression can be separated from true progression [28]. Studies distinguishing pseudoprogression from true progression using imaging biomarkers are emerging, but prospective evaluation is warranted before clinical use [29,30].

Volumetric anatomical assessment is not part of the RANO criteria due to lack of standardization and measurement tool availability [4]. Despite a decrease in CET and an increase in NET volume in all patients during radiochemotherapy, univariate analysis of volumetric change did not separate the two survival groups or predict survival. In a recent study of 125 patients with treatment naïve GBM comparing clinical parameters with MRI parameters, no association ($p = 0.855$) between OS and pre-treatment tumor volume was found [31]. Conversely, Li et al., in a study similar to ours, found a correlation between OS and volume before radiochemotherapy of non-enhancing lesions in 64 patients [32]. While post-surgical tumor volume is a known predictor for OS, extent of resection other than gross-total or sub-total resection is poorly understood [33].

Studies have shown that high $rCBV_{T2}$ may predict shorter OS in GBM patients [34,35]. The DSC-derived parameters $rCBV_{T2}$ and $rCBF_{T2}$ decreased significantly during the radiochemotherapy period, but showed no differences between the two survival groups. One reason for this could be the use of a SE rather than the more commonly used GRE

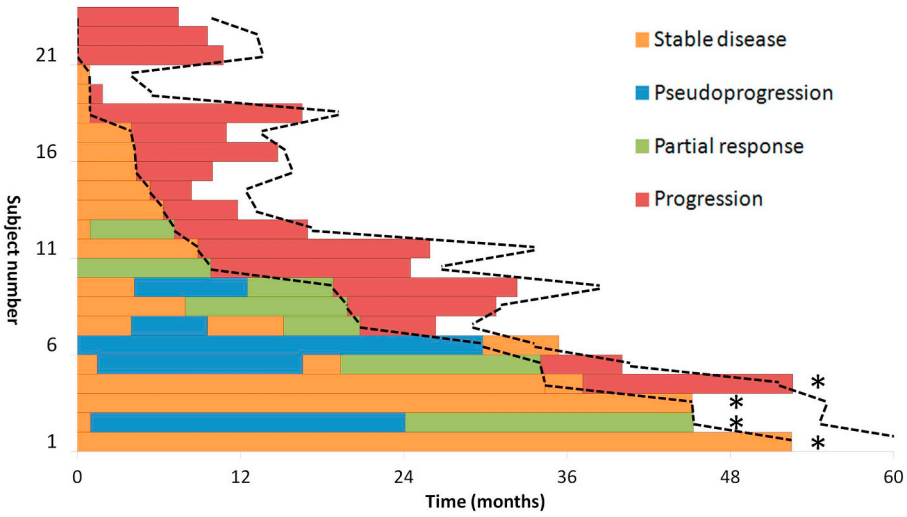

Fig. 1. Event chart for 23 patients sorted by time of radiographic progression. Color represents RANO category, the inner dashed line represents progression-free survival, and the outer dashed line represents overall survival. Subjects still alive at time of analysis are marked with *. The median split was between patient eleven and twelve.

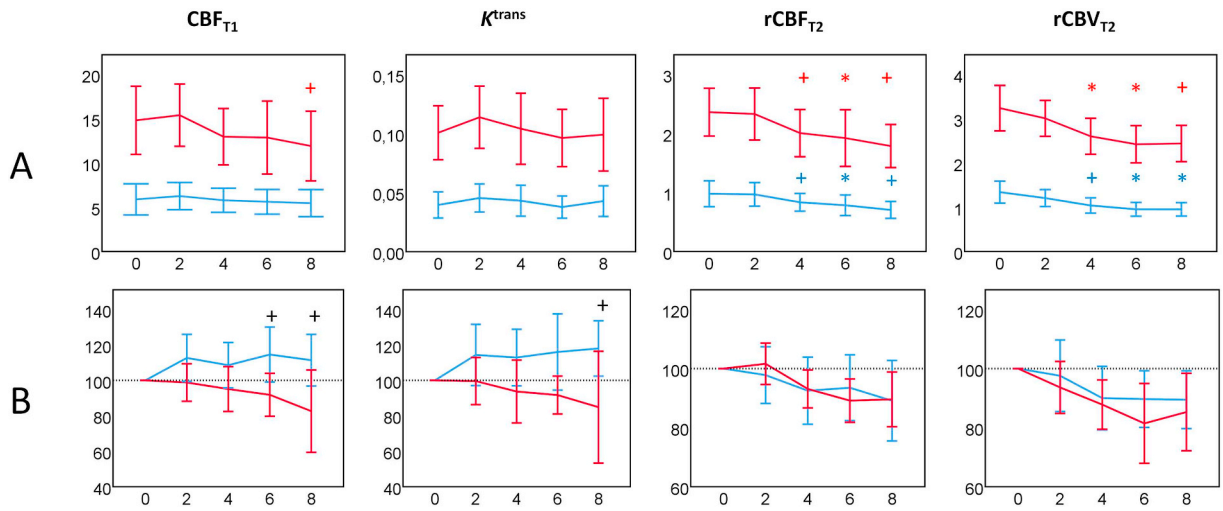

Fig. 2. Temporal trends (top row) and change from baseline (bottom row) in all patients for key parameters from DCE (K^{trans} and CBF_{T1}) and DSC ($rCBF_{T2}$ and $rCBV_{T2}$) in contrast enhancing tumor. In the top row median values are shown in blue and 90 percentile values are shown in red. In the bottom row the blue lines represent subjects with a worse overall survival (OS) and the red lines shows subjects with a better OS based upon the median split groups.
95% confidence intervals are shown at each time point. Significant change from baseline in the upper row or significant difference between the two groups are shown by a plus ($p < 0.05$) or an asterisk ($p < 0.01$). (For interpretation of the references to color in this figure legend, the reader is referred to the web version of this article.)

DSC method. The choice of SE over GRE was based on pilot data showing more artifacts from surgical clips when GRE was used, expected to reduce the number of valid DSC-MRI datasets for analysis. SE generally has a poorer signal-noise-ratio than GRE DSC, due to lower contrast-agent sensitivity, but is at the same time more sensitive to microvascular perfusion [36]. The observed decline in $rCBV_{T2}$ and $rCBF_{T2}$ compared to CBF_{T1} and v_p might therefore reflect a difference in radio-resistance between different-sized blood vessels and auto-regulation of blood flow following damage to capillary endothelial cells [37,38]. Tumoral CBF_{T1} was twice as high as that of apparently unaffected tissue and CBF_{T2} equal to unaffected tissue at therapy start without any group differences. Interestingly, no DSC-based perfusion measures were significantly different between the patient groups, while DCE-derived CBF_{T1} was higher in the subpopulation with the worst prognosis after finishing radiochemotherapy. Simulations looking at shunting in tumor vessels have shown that absence of anti-shunting mechanisms can lead to functional shunting, a condition with high average flow and substantial hypoxia [39]. A lack of anti-shunting mechanisms possibly explains why an increase in CBF_{T1} is associated with a lower-than-average OS. The blood-brain-barrier depends upon the integrity of gap junctions, a signaling pathway propagating the anti-shunting mechanism. The correlation between high K^{trans} and CBF_{T1} might be explained by a higher degree of disruption of these gap-junctions in patients with a poorer prognosis. The decrease in K^{trans} and CBF_{T1} in patients with greater OS could implicate a lesser degree of shunting and normalization of the endothelial integrity in the tumor vessels, a condition thought to promote better effect of anti-cancer therapy [40].

The early overall trend of CBF_{T1} and K^{trans} is in line with previous investigations of perfusion-changes in GBM patients [41]. Møller et al. found, in a study of 11 patients, an increase in CBF_{T1} after one week of radiochemotherapy and a decline in v_p after 5 weeks, similar to our findings. No difference in PFS was found, while other studies have shown that increasing values of K^{trans} is a potential biomarker in early prognostics [8]. Earlier work by Li et al. showed a statistical decrease in $rCBV_{T2}$ and normalized peak height (a biomarker similar to $rCBF_{T2}$) after radiochemotherapy [32]. These results are in good agreement with the results presented here.

The study has limitations. In this study, the extended Tofts model was chosen as the kinetic model for the DCE analysis as this is the

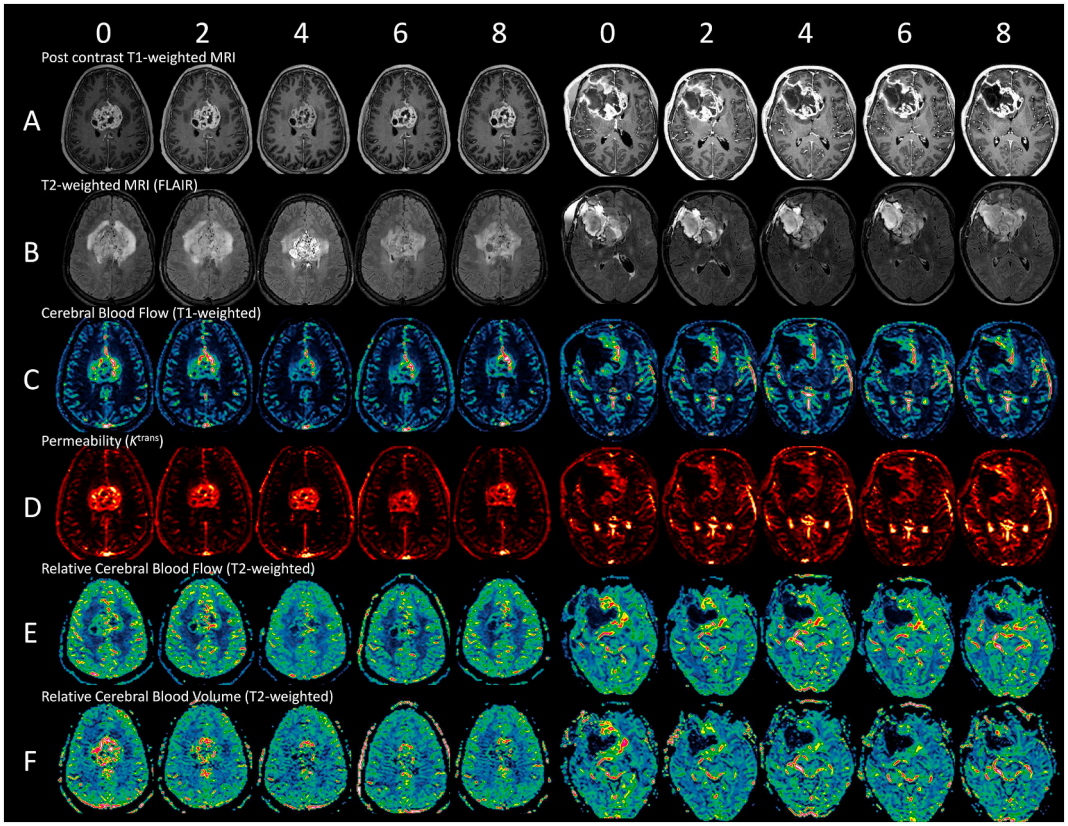

Fig. 3. Representative images from a patient responding to therapy (left) and a non-responding patient (right). (A) T1-w images after injection of gadobutrol. A small size reduction of the CET is seen in the responder. (B) FLAIR images showing high signal around the CET. (C) Maps of DCE-derived CBF showing declining values during and after radiochemotherapy in the responder. In the non-responder increasing flow is noted in the anterior part over the tumor. (D) Maps showing decreasing K^{trans} values in the responder and increasing values in the non-responder. (E) $rCBF_{T2}$ from DSC showing decreasing values typical of all patients. (F) The $rCBV_{T2}$ decreases during therapy to values similar of white matter values.

method most often used in GBM imaging. The chosen method is dependent on the quality of the data and can be assessed by an incremental modeling method [42,43]. This showed that 70% of all tumor voxels were best described using the extended Tofts model in this material. A 'carry-on' AIF approach was implemented, where the patient specific AIF obtained at the baseline scan was used for all subsequent scans. The use of carry-on AIF is based on the assumption that measurement errors in individual AIF measured at each time-point would be larger than the actual patient specific variation in bulk flow to the brain over the eight-week study duration. The improved reproducibility of carry-on AIF over individual AIFs is supported in studies using double baseline data for both DSC and DCE [20,44]. Although the patients received different surgical treatment, no difference in OS or in estimated parameters were found between the different groups. There was, not surprisingly, a difference in CET volume between the groups ($p < 0.003$). However, to remove bias from tumor location and extent of surgery we compared each parameter to the baseline exam and excluded all CET and NET smaller than 0.5 ml. Thus, only temporal evolution of each tumor regardless of these factors was included in the survival index and δ values.

5. Conclusion

Comparing structural and perfusion MRI in GBM patients during radiochemotherapy treatment, temporal changes are more apparent in CET and DSC-derived parameters compared to parameters from DCE. The DCE-derived metrics K^{trans} and CBF_{T1} in CET were found to be the most promising parameters for early OS prediction. A multiparametric approach of change in K^{trans} and $rCBV_{T2}$ shows promise as an early predictor biomarker in this patient group.

Supplementary data to this article can be found online at https://doi.org/10.1016/j.mri.2020.01.012.

Compliance with ethical standards

Author Atle Bjørnerud is a paid consultant of NordicNeuroLab AS. No other conflict of interest was reported from any of the authors.

No funding was received for the writing of this study.

Informed consent from all participants was acquired before imaging according to the ethical region committee and the Helsinki declaration from 1964.

CRediT authorship contribution statement

Christopher Larsson: Conceptualization, Methodology, Software, Validation, Investigation, Resources, Data curation, Writing - original draft, Writing - review & editing, Visualization, Project administration.**Jonas Vardal:**Validation, Investigation, Resources, Data curation, Writing - original draft.**Magne Kleppestø:**Software, Validation, Data curation, Writing - original draft.**Audun Odland:**Investigation, Resources, Data curation, Writing - original draft.**Petter Brandal:**Investigation, Resources, Data curation, Writing - original draft, Supervision.**Paulina Due-Tønnessen:**Investigation, Resources, Data curation, Writing - original draft, Supervision.**Sigrun S. Holme:**Investigation, Resources, Data curation, Writing - original draft.**Tuva R. Hope:**Validation, Resources, Data curation, Writing - original draft.**Torstein R. Meling:**Investigation, Data curation, Writing - original draft, Supervision.**Erik Fosse:**Resources, Data curation, Writing - original draft, Supervision, Funding acquisition.**Kyrre E.**

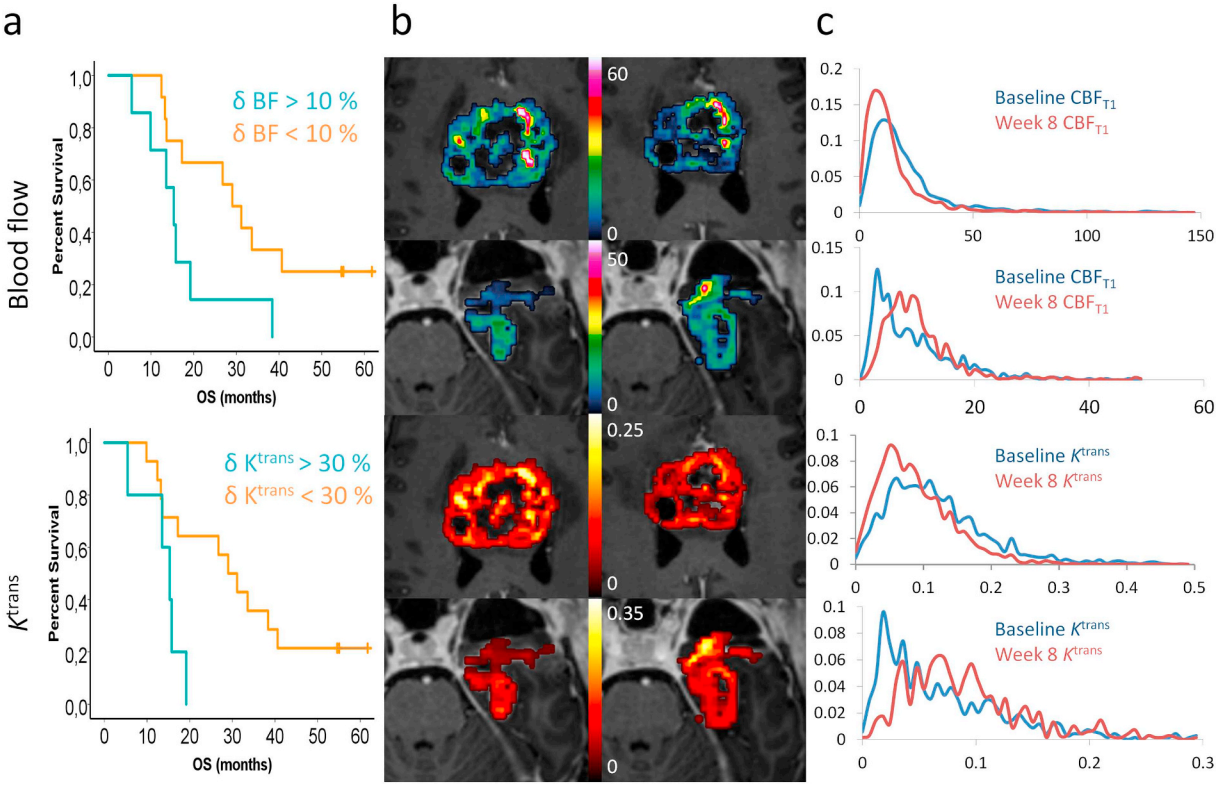

Fig. 4. (A) Kaplan-Meier plots dividing patients according CBF and K^{trans} cut-offs. An increase in K^{trans} and CBF <30% and 10% at eight weeks from baseline, respectively, predicted longer survival. (B) Example of change in parameter maps of CBF and K^{trans} in two sample patients with large difference in OS. (C) Respective changes in histogram distribution of each parameter from baseline (blue) to eight weeks (red) for the same two sample patients. (For interpretation of the references to color in this figure legend, the reader is referred to the web version of this article.)

Emblem: Conceptualization, Methodology, Validation, Formal analysis, Resources, Data curation, Writing - original draft, Writing - review & editing, Visualization.**Atle Bjørnerud:**Conceptualization, Methodology, Software, Validation, Formal analysis, Investigation, Resources, Data curation, Writing - original draft, Writing - review & editing, Visualization, Supervision, Project administration, Funding acquisition.

Acknowledgments

The authors would like to thank radiographers Grethe Løvland, Svein Are Vatnehol and Terje Tillung for invaluable help.

References

[1] Helseth R, Helseth E, Johannesen TB, Langberg CW, Lote K, Rønning P, et al. Overall survival, prognostic factors, and repeated surgery in a consecutive series of 516 patients with glioblastoma multiforme. Acta Neurol Scand 2010;122:159–67. https://doi.org/10.1111/j.1600-0404.2010.01350.x.

[2] Stupp R, Mason W, van den Bent MJ, Weller M, Fisher BM, Taphoorn MJB, et al. Radiotherapy plus concomitant and adjuvant temozolomide for glioblastoma. N Engl J Med 2005;352:987–96. https://doi.org/10.1056/NEJMoa043330.

[3] Kiely BE, Tattersall MHN, Stockler MR. Certain death in uncertain time: informing hope by quantifying a best case scenario. J Clin Oncol 2010;28:2802–4. https://doi.org/10.1200/JCO.2009.27.3326.

[4] Wen PY, Macdonald DR, Reardon DA, Cloughesy TF, Sorensen AG, Galanis E, et al. Updated response assessment criteria for high-grade gliomas: response assessment in neuro-oncology working group. J Clin Oncol 2010;28:1963–72. https://doi.org/10.1200/JCO.2009.26.3541.

[5] Reuter M, Gerstner ER, Rapalino O, Batchelor TT, Rosen B, Fischl B. Impact of MRI head placement on glioma response assessment. J Neurooncol 2014;118:123–9. https://doi.org/10.1007/s11060-014-1403-8.

[6] Kalpathy-Cramer J, Gerstner ER, Emblem KE, Andronesi OC, Rosen B. Advanced magnetic resonance imaging of the physical processes in human Glioblastoma. Cancer Res 2014;74:4622–37. https://doi.org/10.1158/0008-5472.CAN-14-0383.

[7] Dickerson E, Srinivasan A. Multicenter survey of current practice patterns in perfusion MRI in neuroradiology: why, when, and how is it performed? Am J Roentgenol 2016;207:406–10. https://doi.org/10.2214/AJR.15.15740.

[8] Nguyen TB, Cron GO, Mercier JF, Foottit C, Torres CH, Chakraborty S, et al. Preoperative prognostic value of dynamic contrast-enhanced MRI-derived contrast transfer coefficient and plasma volume in patients with cerebral gliomas. Am J Neuroradiol 2015;36:63–9. https://doi.org/10.3174/ajnr.A4006.

[9] Law M, Young RJ, Babb JS, Peccerelli N, Chheang S, Gruber ML, et al. Gliomas: predicting time to progression or survival with cerebral blood volume measurements at dynamic susceptibility-weighted contrast-enhanced perfusion MR imaging. Radiology 2008;247:490–8. https://doi.org/10.1148/radiol.2472070898.

[10] Bonekamp D, Deike K, Wiestler B, Wick W, Bendszus M, Radbruch A, et al. Association of overall survival in patients with newly diagnosed glioblastoma with contrast-enhanced perfusion MRI: comparison of intraindividually matched T<inf>1</inf>− and T<inf>2</inf>−based bolus techniques. J Magn Reson Imaging 2015;42:87–96. https://doi.org/10.1002/jmri.24756.

[11] Emblem KE, Farrar CT, Gerstner ER, Batchelor TT, Borra RJH, Rosen BR, et al. Vessel calibre—a potential MRI biomarker of tumour response in clinical trials. Nat Rev Clin Oncol 2014;11:566–84. https://doi.org/10.1038/nrclinonc.2014.126.

[12] Karnofsky DA, Abelmann WH, Craver LF, Burchenal JH. The use of the nitrogen mustards in the palliative treatment of carcinoma. With particular reference to bronchogenic carcinoma. Cancer 1948;1:634–56. https://doi.org/10.1002/1097-0142(194811)1:4<634::AID-CNCR2820010410>3.0.CO;2-L.

[13] Larsson HBW, Courivaud F, Rostrup E, Hansen AE. Measurement of brain perfusion, blood volume, and blood-brain barrier permeability, using dynamic contrast-enhanced T_1-weighted MRI at 3 tesla. Magn Reson Med 2009;62:1270–81. https://doi.org/10.1002/mrm.22136.

[14] Kleppestø M, Larsson C, Groote I, Salo R, Vardal J, Courivaud F, et al. T2*-correction in dynamic contrast-enhanced MRI from double-echo acquisitions. J Magn Reson Imaging 2014;39:1314–9. https://doi.org/10.1002/jmri.24268.

[15] Odland A, Server A, Saxhaug C, Breivik B, Groote R, Vardal J, et al. Volumetric glioma quantification: comparison of manual and semi-automatic tumor segmentation for the quantification of tumor growth. Acta Radiol 2015;56:1396–403. https://doi.org/10.1177/0284185114554822.

[16] Majós C, Cos M, Castañer S, Gil M, Plans G, Lucas A, et al. Early post-operative magnetic resonance imaging in glioblastoma: correlation among radiological findings and overall survival in 60 patients. Eur Radiol 2016;26:1048–55. https://doi.org/10.1007/s00330-015-3914-x.

[17] Tofts PS, Brix G, Buckley DL, Evelhoch JL, Henderson E, Knopp MV, et al. Estimating kinetic parameters from dynamic contrast-enhanced T1-weighted MRI of a diffusable tracer: standardized quantities and symbols. J Magn Reson Imaging 1999;10:223–32. https://doi.org/10.1002/(SICI)1522-2586(199909)10:3<223::AID-JMRI2>3.0.CO;2-S.

[18] Haacke EM, Filleti CL, Gattu R, Ciulla C, Al-Bashir A, Suryanarayanan K, et al. New

algorithm for quantifying vascular changes in dynamic contrast-enhanced MRI independent of absolute T1 values. Magn Reson Med 2007;58:463–72. https://doi.org/10.1002/mrm.21358.
[19] Larsson C, Kleppestø M, Bjørnerud A. Investigation of the necessity of pre-contrast T1-determination in DCE MRI; simulations and clinical data. Proc Intl Soc Mag Reson Med 2013;3:5236.
[20] Mouridsen K, Emblem KE, Bjørnerud A, Jennings D, Sorensen AG. Subject-specific AIF optimizes reproducibility of perfusion parameters in longitudina l DSC-MRI in comparison to session and population level AIF. Proc. Intl. Soc. Mag. Reson. Med, Montreal. 2011.
[21] Holland D, Kuperman JM, Dale AM. Efficient correction of inhomogeneous static magnetic field-induced distortion in echo planar imaging. Neuroimage 2010;50:175–83. https://doi.org/10.1016/j.neuroimage.2009.11.044.
[22] Østergaard L, Sorensen AG, Kwong KK, Weisskoff RM, Gyldensted C, Rosen BR. High resolution measurement of cerebral blood flow using intravascular tracer bolus passages. Part II: experimental comparison and preliminary results. Magn Reson Med 1996;36:726–36. https://doi.org/10.1002/mrm.1910360511.
[23] Bjørnerud A, Emblem KE. A fully automated method for quantitative cerebral hemodynamic analysis using DSC–MRI. J Cereb Blood Flow Metab 2010;30:1066–78. https://doi.org/10.1038/jcbfm.2010.4.
[24] Østergaard L, Weisskoff RM, Chesler DA, Gyldensted C, Rosen BR. High resolution measurement of cerebral blood flow using intravascular tracer bolus passages. Part I: mathematical approach and statistical analysis. Magn Reson Med 1996;36:715–25. https://doi.org/10.1002/mrm.1910360510.
[25] Youden WJ. Index for rating diagnostic tests. Cancer 1950;3:32–5. https://doi.org/10.1002/1097-0142(1950)3:1<32::AID-CNCR2820030106>3.0.CO;2-3.
[26] Sorensen AG, Batchelor TT, Zhang WT, Chen PJ, Yeo P, Wang M, et al. A "vascular normalization index" as potential mechanistic biomarker to predict survival after a single dose of cediranib in recurrent glioblastoma patients. Cancer Res 2009;69:5296–300. https://doi.org/10.1158/0008-5472.CAN-09-0814.
[27] Pencina MJ, D'Agostino RB. OverallC as a measure of discrimination in survival analysis: model specific population value and confidence interval estimation. Stat Med 2004;23:2109–23. https://doi.org/10.1002/sim.1802.
[28] Brandsma D, Stalpers L, Taal W, Sminia P, van den Bent MJ. Clinical features, mechanisms, and management of pseudoprogression in malignant gliomas. Lancet Oncol 2008;9:453–61. https://doi.org/10.1016/S1470-2045(08)70125-6.
[29] Cha J, Kim ST, Kim HJ, Kim BJ, Kim YK, Lee JY, et al. Differentiation of tumor progression from pseudoprogression in patients with posttreatment glioblastoma using multiparametric histogram analysis. Am J Neuroradiol 2014;35:1309–17. https://doi.org/10.3174/ajnr.A3876.
[30] Thomas AA, Arevalo-Perez J, Kaley T, Lyo J, Peck KK, Shi W, et al. Dynamic contrast enhanced T1 MRI perfusion differentiates pseudoprogression from recurrent glioblastoma. J Neurooncol 2015;125:183–90. https://doi.org/10.1007/s11060-015-1893-z.
[31] Burth S, Kickingereder P, Eidel O, Tichy D, Bonekamp D, Weberling L, et al. Clinical parameters outweigh diffusion- and perfusion-derived MRI parameters in predicting survival in newly diagnosed glioblastoma. Neuro Oncol 2016;18:1673–9. https://doi.org/10.1093/neuonc/now122.
[32] Li Y, Lupo JM, Polley M-Y, Crane JC, Bian W, Cha S, et al. Serial analysis of imaging parameters in patients with newly diagnosed glioblastoma multiforme. Neuro Oncol 2011;13:546–57. https://doi.org/10.1093/neuonc/noq194.
[33] Brown TJ, Brennan MC, Li M, Church EW, Brandmeir NJ, Rakszawski KL, et al. Association of the extent of resection with survival in glioblastoma. JAMA Oncol 2016;2:1460. https://doi.org/10.1001/jamaoncol.2016.1373.
[34] Coban G, Mohan S, Kural F, Wang S, O'Rourke DM, Poptani H. Prognostic value of dynamic susceptibility contrast-enhanced and diffusion-weighted MR imaging in patients with glioblastomas. AJNR Am J Neuroradiol 2015;36:1247–52. https://doi.org/10.3174/ajnr.A4284.
[35] Jain R, Poisson LM, Gutman D, Scarpace L, Hwang SN, Holder CA, et al. Outcome prediction in patients with glioblastoma by using imaging, clinical, and genomic biomarkers: focus on the nonenhancing component of the tumor. Radiology 2014;272:484–93. https://doi.org/10.1148/radiol.14131691.
[36] Boxerman JL, Hamberg LM, Rosen BR, Weisskoff RM. Mr contrast due to intravascular magnetic susceptibility perturbations. Magn Reson Med 1995;34:555–66. https://doi.org/10.1002/mrm.1910340412.
[37] Petr J, Platzek I, Seidlitz A, Mutsaerts HJMM, Hofheinz F, Schramm G, et al. Early and late effects of radiochemotherapy on cerebral blood flow in glioblastoma patients measured with non-invasive perfusion MRI. Radiother Oncol 2016;118:24–8. https://doi.org/10.1016/j.radonc.2015.12.017.
[38] O'Connor MM, Mayberg MR. Effects of radiation on cerebral vasculature: a review. Neurosurgery 2000;46:138–51. https://doi.org/10.1016/j.wneu.2014.01.006.
[39] Pries AR, Höpfner M, le Noble F, Dewhirst MW, Secomb TW. The shunt problem: control of functional shunting in normal and tumour vasculature. Nat Rev Cancer 2010;10:587–93. https://doi.org/10.1038/nrc2895.
[40] Jain RK. Normalizing tumor vasculature with anti-angiogenic therapy: a new paradigm for combination therapy. Nat Med 2001;7:987–9. https://doi.org/10.1038/nm0901-987.
[41] Møller S, Lundemann M, Law I, Poulsen HS, Larsson HBW, Engelholm SA. Early changes in perfusion of glioblastoma during radio- and chemotherapy evaluated by T1-dynamic contrast enhanced magnetic resonance imaging. Acta Oncol (Madr) 2015;54:1521–8. https://doi.org/10.3109/0284186X.2015.1063777.
[42] Bagher-Ebadian H, Jain R, Nejad-Davarani SP, Mikkelsen T, Lu M, Jiang Q, et al. Model selection for DCE-T1 studies in glioblastoma. Magn Reson Med 2012;68:241–51. https://doi.org/10.1002/mrm.23211.
[43] Sourbron SP, Buckley DL. Classic models for dynamic contrast-enhanced MRI. NMR Biomed 2013;26:1004–27. https://doi.org/10.1002/nbm.2940.
[44] Larsson C, Kalpathy-Cramer J, Bjørnerud A, Wen PY, Batchelor TT, Jain RK, et al. Re-use of subject-specific AIFs are warranted in longitudinal DCE-MRI. Proc. ISMRM. 10. 2014. p. 6408.